

Scaling behavior of quark propagator in full QCD

Maria B. Parappilly¹, Patrick O. Bowman², Urs M. Heller³,
Derek B. Leinweber¹, Anthony G. Williams¹ and J. B. Zhang¹

¹ *Special Research Center for the Subatomic Structure of Matter (CSSM)
and Department of Physics, University of Adelaide 5005, Australia*

² *Nuclear Theory Center, Indiana University, Bloomington IN 47405, USA*

³ *American Physical Society, One Research Road, Box 9000, Ridge, NY 11961-9000, USA*

(Dated: August 28, 2017)

We study the scaling behavior of the quark propagator on two lattices with similar physical volume in Landau gauge with 2+1 flavors of dynamical quarks in order to test whether we are close to the continuum limit for these lattices. We use configurations generated with an improved staggered (“Asqtad”) action by the MILC collaboration. The calculations are performed on $28^3 \times 96$ lattices with lattice spacing $a = 0.09$ fm and on $20^3 \times 64$ lattices with lattice spacing $a = 0.12$ fm. We calculate the quark mass function, $M(q^2)$, and the wave-function renormalization function, $Z(q^2)$, for a variety of bare quark masses. Comparing the behavior of these functions on the two sets of lattices we find that both $Z(q^2)$ and $M(q^2)$ show little sensitivity to the ultraviolet cutoff.

PACS numbers: 12.38.Gc 11.15.Ha 12.38.Aw 14.65.-q

I. INTRODUCTION

Quantum Chromodynamics (QCD) is widely considered to be the correct theory of the strong interactions. Quarks and gluons are the fundamental degrees of freedom of this theory. The quark propagator contains valuable information about nonperturbative QCD. The systematic study of the quark propagator on the lattice has provided fruitful interaction with other approaches to hadron physics, such as instanton phenomenology [1], chiral quark models [2] and Dyson-Schwinger equation studies [3, 4]. As a first principles approach lattice QCD has provided valuable constraints for model builders. In turn, such alternative methods can provide feedback on regions that are difficult to access directly on the lattice, such as the deep infrared and chiral limits.

The quark propagator has previously been studied using Clover [5, 6], staggered [7, 8] and Overlap [9, 10, 11] actions. For a review, see Ref. [12]. All these actions have different systematic errors and the combination of these studies has given us an excellent handle on the possible lattice artifacts in quenched QCD.

In this study we focus on the Landau gauge quark propagator in full QCD, and extend our previous work [13] to a finer lattice with lattice spacing $a = 0.09$ fm [14] but similar physical volume in order to test whether we are close to the continuum limit for these lattices. The scaling behavior of the momentum space quark propagator is examined by comparing the results on these two lattices. Our results show that there are no significant differences in the wave-function renormalization function and quark mass function on the two sets of lattices. Therefore the scaling behavior is good already at the coarser lattice spacing of $a = 0.12$ fm.

The configurations we use in this study were generated by the MILC collaboration [14, 15] and are available from the Gauge Connection [16]. The dynamical configurations have two degenerate light fermions for the

u and d quarks and a heavier one for the strange quark. Weighting for the fermion determinants is provided by the so-called, “fourth root trick.” While the current numerical results [17] provide compelling evidence that the fourth root trick gives an accurate estimate of the dynamical fermion weight, the formal issue of proving that this provides the determinant of a local fermion action from first principles remains unresolved.

II. DETAILS OF THE CALCULATION

The quark propagator is gauge dependent and we work in the Landau gauge for ease of comparison with other studies. Landau gauge is a smooth gauge that preserves the Lorentz invariance of the theory, so it is a popular choice. As derived in Ref. [18] an improved Landau-gauge-fixing functional, $\mathcal{F}_{\text{Imp}}^G \equiv \frac{4}{3}\mathcal{F}_1^G - \frac{1}{12u_0}\mathcal{F}_2^G$ is used where

$$\mathcal{F}_1^G[\{U\}] = \sum_{\mu,x} \frac{1}{2} \text{Tr} \{U_\mu^G(x) + U_\mu^G(x)^\dagger\}, \quad (1)$$

$$\mathcal{F}_2^G = \sum_{x,\mu} \frac{1}{2} \text{Tr} \{U_\mu^G(x)U_\mu^G(x + \hat{\mu}) + \text{h.c.}\}. \quad (2)$$

$$U_\mu^G(x) = G(x)U_\mu(x)G(x + \hat{\mu})^\dagger, \quad (3)$$

$$G(x) = \exp \left\{ -i \sum_a \omega^a(x) T^a \right\}, \quad (4)$$

and u_0 is the plaquette measure of the mean link. We adopt a “steepest descents” approach. The functional

derivative of $\mathcal{F}_{\text{Imp}}^G$ with respect to ω^a provide

$$\Delta_1(x) \equiv \frac{1}{u_0} \sum_{\mu} [U_{\mu}(x - \mu) - U_{\mu}(x) - \text{h.c.}]_{\text{traceless}} \quad (5)$$

$$\Delta_2(x) \equiv \frac{1}{u_0^2} \sum_{\mu} \left[U_{\mu}(x - 2\mu)U_{\mu}(x - \mu) - U_{\mu}(x)U_{\mu}(x + \mu) - \text{h.c.} \right]_{\text{traceless}} \quad (6)$$

and

$$\Delta_{\text{Imp}}(x) \equiv \frac{4}{3}\Delta_1(x) - \frac{1}{12}\Delta_2(x). \quad (7)$$

The resulting gauge transformation is

$$G_{\text{Imp}}(x) = \exp \left\{ \frac{\alpha}{2} \Delta_{\text{Imp}}(x) \right\}, \quad (8)$$

where α is a tuneable step-size parameter. The gauge fixing algorithm proceeds by calculating the relevant Δ_i in terms of the mean-field-improved links, and then applying the associated gauge transformation, Eq. (8), to the gauge field. The algorithm using conjugate gradient Fourier acceleration is implemented in parallel, updating all links simultaneously, and is iterated until the Lattice Landau gauge condition

$$\theta_{\text{Imp}} = \frac{1}{VN_c} \sum_x \text{Tr} \{ \Delta_{\text{Imp}}(x) \Delta_{\text{Imp}}(x)^{\dagger} \} \quad (9)$$

is satisfied with accuracy of $\theta_i < 10^{-12}$.

As this gauge fixing finds a local minimum of the gauge fixing functional, we are necessarily sampling from the first Gribov region. Our ensemble contains no gauge-equivalent configurations and hence has no Gribov copies as such. However, our configurations are local minima and *absolute* minima and therefore are not from the Fundamental Modular Region [19]. It is known from previous $SU(3)$ studies that neither the gluon nor quark propagator display any obvious Gribov noise above and beyond the ensemble statistical noise and so we do not consider it further here [20, 21, 22]. It will be interesting to repeat this calculation for the Gribov-copy free Laplacian gauge, and to do a systematic search for Gribov noise in Landau gauge, but these are left for future studies.

The MILC configurations were generated with the $\mathcal{O}(a^2)$ one-loop Symanzik-improved Lüscher–Weisz gauge action [23]. The dynamical configurations use the Asqtad quark action [24], an $\mathcal{O}(a^2)$ Symanzik-improved staggered fermion action which removes lattice artifacts up to order $a^2 g^2$. We refer to the $a = 0.09$ fm lattice as the “fine” lattice and the $a = 0.12$ fm one as the “coarse” lattice.

We explore two light sea quark masses, $ma = 0.0062$ ($m = 14.0$ MeV) and $ma = 0.0124$ ($m = 27.1$ MeV). The

TABLE I: Lattice parameters used in this study. The dynamical configurations each have two degenerate light quarks (up/down) and a heavier quark (strange). The light bare quark masses for the $28^3 \times 96$ lattice are 14.0 MeV and 27.1 MeV with a strange quark mass of 67.8 MeV. For the $20^3 \times 64$ lattice the bare quark masses range from 15.7 MeV to 78.9 MeV. The lattice spacing is $a \simeq 0.12$ fm for the $20^3 \times 64$ lattice and $a \simeq 0.09$ fm [14] for the $28^3 \times 96$ lattice.

	Dimensions	β	a	Bare Quark Mass	# Config
1	$28^3 \times 96$	7.09	0.086 fm	14.0 MeV, 67.8 MeV	108
2	$28^3 \times 96$	7.11	0.086 fm	27.1 MeV, 67.8 MeV	110
3	$20^3 \times 64$	6.76	0.121 fm	15.7 MeV, 78.9 MeV	203
4	$20^3 \times 64$	6.79	0.121 fm	31.5 MeV, 78.9 MeV	249
5	$20^3 \times 64$	6.81	0.120 fm	47.3 MeV, 78.9 MeV	268
6	$20^3 \times 64$	6.83	0.119 fm	63.1 MeV, 78.9 MeV	318

bare strange quark mass was fixed at $ma = 0.031$, or $m = 67.8$ MeV for $a = 0.09$ fm. The values of the coupling and the bare light sea-quark masses are matched such that the lattice spacing is held constant. The simulation parameters are summarized in Table I with the lattice spacings taken from [14].

On the lattice, the bare propagator $S(a; p^2)$ is related to the renormalized propagator $S^{\text{ren}}(\mu; p^2)$ through the renormalization constant [13]

$$S(a; p^2) = Z_2(a; \mu) S^{\text{ren}}(\mu; p^2). \quad (10)$$

In the continuum limit, Lorentz invariance allows one to decompose the full quark propagator into Dirac vector and scalar pieces

$$S^{-1}(p^2) = Z^{-1}(p^2) [i\gamma \cdot p + M(p^2)], \quad (11)$$

where $M(p^2)$ and $Z(p^2)$ are the nonperturbative mass and wave function renormalization functions, respectively. Asymptotic freedom implies that, as $p^2 \rightarrow \infty$, $S(p^2)$ reduces to the tree-level propagator

$$S^{-1}(p^2) \rightarrow i\gamma \cdot p + m, \quad (12)$$

up to logarithmic corrections. The mass function M is renormalization point independent and for Z we choose throughout this work the renormalization point as $\mu = 3.0$ GeV, *i.e.*,

$$S^{\text{ren}}(\mu; \mu^2) = \frac{S(a; \mu^2)}{Z_2(a; \mu)} = 1, \quad (13)$$

thus defining $Z_2(a; \mu)$.

The tree-level quark propagator with the Asqtad action has the form

$$S^{-1}(p) = i \sum_{\mu} \vec{\gamma}_{\mu} q(p_{\mu}) + m, \quad (14)$$

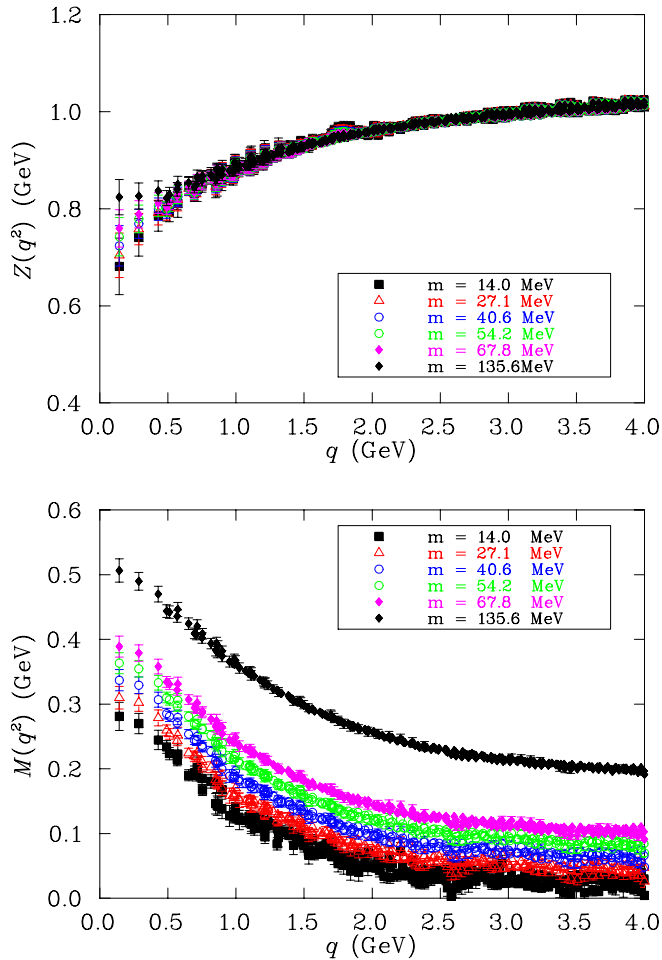


FIG. 1: The unquenched wave-function renormalization function $Z(q^2)$ and mass function $M(q^2)$ for a variety of valence quark masses (shown in the inset), with the light sea-quark mass fixed at $m = 14.0$ MeV. The renormalization function is renormalized at $q = 3.0$ GeV.

where $q(p_\mu)$ is the kinematic momentum given in [7]

$$q_\mu \equiv \sin(p_\mu) \left[1 + \frac{1}{6} \sin^2(p_\mu) \right]. \quad (15)$$

The $\bar{\gamma}_\mu$ form a staggered Dirac algebra (see Eq.(A.6) and (A.7) of Ref. [13]). Having identified the kinematic momentum, we define the mass and renormalization functions by

$$S^{-1}(p) = Z^{-1}(q) \left[i \sum_\mu (\bar{\gamma}_\mu) q_\mu(p_\mu) + M(q) \right]. \quad (16)$$

Additional details can be found in Ref. [13]

III. NUMERICAL RESULTS

In Fig. 1 we show the results for the mass function $M(q^2)$ and wave-function renormalization function $Z(q^2)$

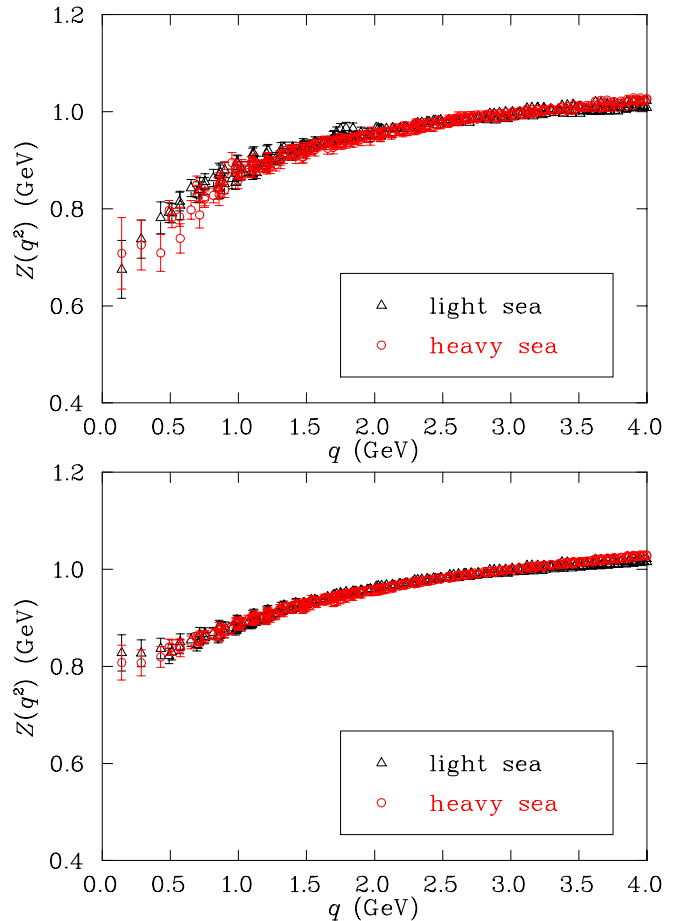


FIG. 2: The unquenched wave-function renormalisation function for the two different values of the light sea quark mass on the fine lattice (14.0 MeV and 27.1 MeV). The valence quark masses are $m = 14.0$ MeV (top) and $m = 135.6$ MeV (bottom), the lightest and heaviest in our current sample respectively. The renormalization function is renormalized at $q = 3.0$ GeV.

for the lightest of our light sea quark masses for a variety of valence quark masses. In these figures, one valence quark mass (14.0 MeV) is identical to the light sea quark mass, as in full QCD. The others are partially quenched results. The data are ordered as we expect, i.e., the larger the bare valence quark mass, the higher $M(q^2)$. The wave-function renormalization function, $Z(q^2)$, on the other hand, is infrared suppressed and the smaller the valence quark mass, the more pronounced the dip at low momenta. In Figs. 2 and 3 we instead hold the valence quark mass fixed and vary the sea quark mass. Clearly the dependence over this small range of sea quark masses is weak. Unfortunately we only have two dynamical sets to compare, and for the lightest valence quark the data are rather noisy.

Next we work on two lattices with different lattice spacing but similar physical volume. We compare the wave-function renormalization function $Z(q^2)$ and mass

function $M(q^2)$ for two lattices with different lattice spacing a in full lattice QCD.

In Fig. 4, we show the quark propagator from the fine lattice for full QCD (light sea-quark mass and valence quark mass equal) with the light quark mass set to $m = 27.1$ MeV. This is compared with data from the coarse lattice by a simple linear interpolation from the four different data sets so the running masses are the same at $q^2 = 3.0$ GeV. Fig. 5 repeats this for the lighter sea quark, $m = 14.0$ MeV. The quark propagators are in excellent agreement, showing no dependence on the lattice spacing.

IV. CONCLUSIONS

In this study we performed a systematic comparison of the Asqtad quark propagator in full QCD for two lattices

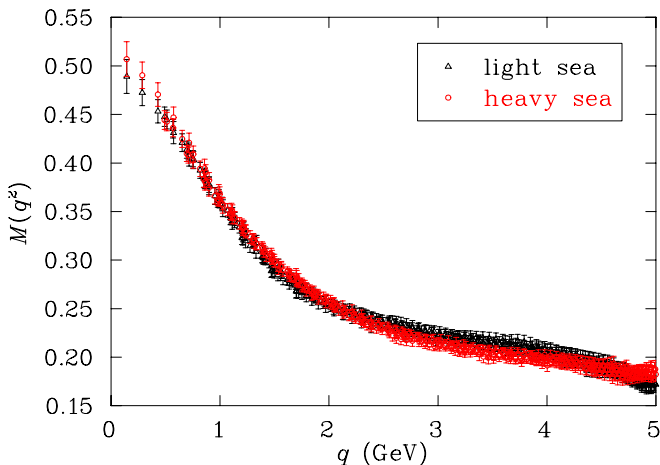
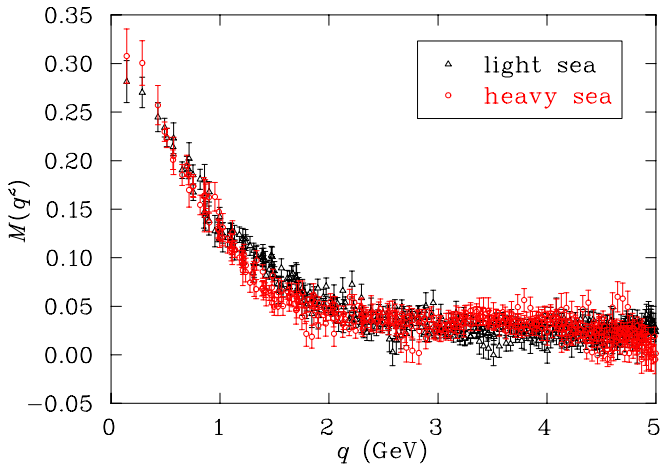


FIG. 3: The unquenched quark mass function for the two different values of the light sea quark mass on the fine lattice (14.0 MeV and 27.1 MeV). The valence quark masses are $m = 14.0$ MeV (top) and $m = 135.6$ MeV (bottom), the lightest and heaviest in our current sample respectively.

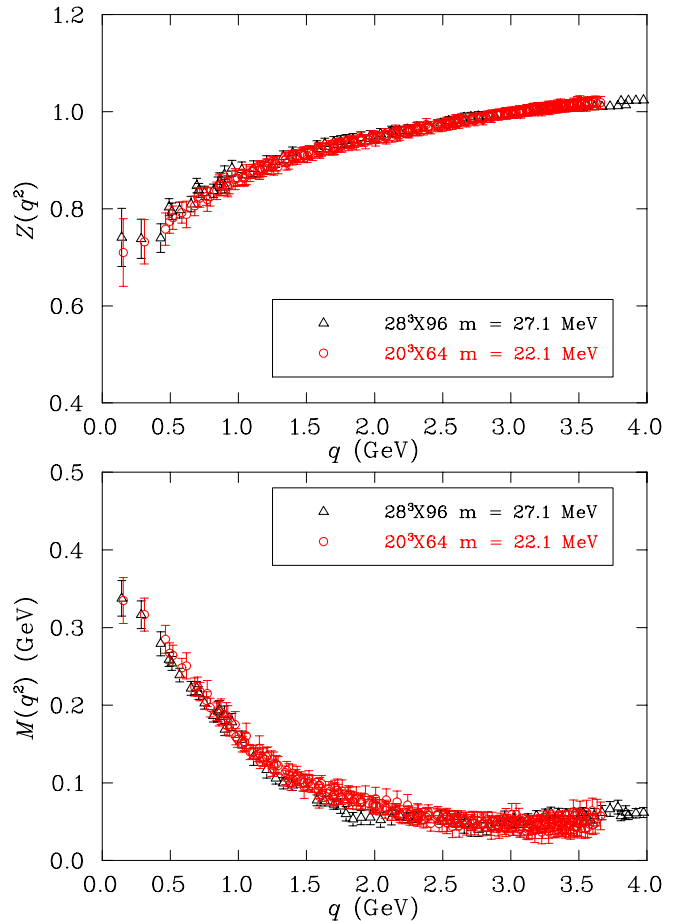


FIG. 4: Comparison of wave-function renormalization function $Z(q^2)$ and mass function $M(q^2)$ for two different lattices. Triangles correspond to the quark propagator at mass $m = 27.1$ MeV from $28^3 \times 96$ with lattice spacing $a = 0.09$ fm. The open circles are the data from $20^3 \times 64$ with lattice spacing $a = 0.12$ fm obtained by interpolating four different set of light quark masses making the $M(q^2)$ value matched for both lattices at $q = 3.0$ GeV. The renormalization point for $Z(q^2)$ is set at $q = 3.0$ GeV for both lattices.

with different lattice spacing in order to establish how close these lattices are to the scaling region and hence to the continuum limit. We compared the two functions $Z(q^2)$ and $M(q^2)$ on fine and coarse lattices and found them to be consistent within errors. We can thus deduce that for both lattices we are close to the scaling region for the quark propagator, which for example makes these lattices suitable for future studies attempting to determine quark masses [25].

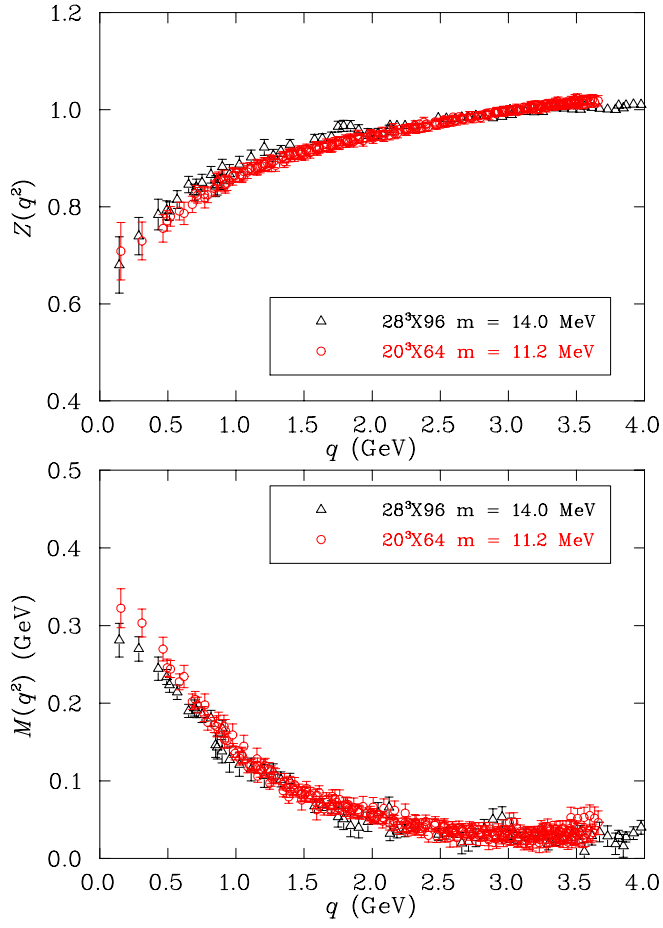


FIG. 5: This figure is same as figure 3, except the light quark mass of $28^3 \times 96$ with lattice spacing $a = 0.09$ fm is $m = 14.0$ MeV. The renormalization point for $Z(q^2)$ is set at $q = 3.0$ GeV for both lattices.

ACKNOWLEDGMENTS

We thank the Australian Partnership for Advanced Computing (APAC) and the South Australian Partnership for Advanced Computing (SAPAC) for generous

grants of supercomputer time which have enabled this project. POB thanks the CSSM for its hospitality during part of this work. This work is supported by the Australian Research Council.

-
- [1] D. Diakonov, *Prog. Part. Nucl. Phys.* **51**, 173 (2003), hep-ph/0212026.
- [2] E. Ruiz Arriola and W. Broniowski, *Phys. Rev.* **D67**, 074021 (2003), hep-ph/0301202.
- [3] M. S. Bhagwat, M. A. Pichowsky, C. D. Roberts, and P. C. Tandy, *Phys. Rev.* **C68**, 015203 (2003), nucl-th/0304003.
- [4] R. Alkofer, W. Detmold, C. S. Fischer, and P. Maris, *Phys. Rev.* **D70**, 014014 (2004), hep-ph/0309077.
- [5] J. I. Skullerud and A. G. Williams, *Phys. Rev.* **D63**, 054508 (2001), hep-lat/0007028.
- [6] J. Skullerud, D. B. Leinweber, and A. G. Williams, *Phys. Rev.* **D64**, 074508 (2001), hep-lat/0102013.
- [7] P. O. Bowman, U. M. Heller, and A. G. Williams, *Phys. Rev.* **D66**, 014505 (2002), hep-lat/0203001.
- [8] P. O. Bowman, U. M. Heller, D. B. Leinweber, and A. G. Williams, *Nucl. Phys. Proc. Suppl.* **119**, 323 (2003), hep-lat/0209129.
- [9] F. D. R. Bonnet, P. O. Bowman, D. B. Leinweber, A. G. Williams, and J. B. Zhang, *Phys. Rev.* **D65**, 114503 (2002), hep-lat/0202003.
- [10] J. B. Zhang, F. D. R. Bonnet, P. O. Bowman, D. B. Leinweber, A. G. Williams, *Phys. Rev.* **D70**, 034505 (2004), hep-lat/0301018.
- [11] P. Boucaud *et al.*, *Phys. Lett. B* **575**, 256 (2003) [arXiv:hep-lat/0307026].
- [12] P. O. Bowman, U. M. Heller, D. B. Leinweber, A. G. Williams, and J. B. Zhang, Quark propagator from LQCD and its physical implications, in *Lattice Hadron Physics*, Lecture Notes in Physics, Springer-Verlag (2005).
- [13] P. O. Bowman, U. M. Heller, D. B. Leinweber, M. B. Parappilly, A. G. Williams, and J. B. Zhang, *Phys. Rev.* **D71**, 054507 (2005), hep-lat/0501019.
- [14] C. Aubin *et al.*, *Phys. Rev.* **D70**, 094505 (2004), hep-lat/0402030.
- [15] C. W. Bernard *et al.*, *Phys. Rev.* **D64**, 054506 (2001), hep-lat/0104002.
- [16] NERSC, Gauge connection, <http://www.qcd-dmz.nersc.gov>.
- [17] S. Dürr PoS **LAT2005**, 021 (2005), hep-lat/0509026.
- [18] F. D. R. Bonnet *et al.*, *Austral. J. Phys.* **52**, 939-948 (1999), hep-lat/9905006.
- [19] A. G. Williams, *Nucl. Phys. Proc. Suppl.* **109A**, 141-145 (2002), hep-lat/0202010.
- [20] L. Giusti, M. L. Paciello, S. Petrarca, B. Taglienti, and N. Tantalo, *Nucl. Phys. Proc. Suppl.* **106**, 995-997 (2002), hep-lat/0110040.
- [21] A. Sternbeck, E. -M. Ilgenfritz, M. Müller-Preussker, and A. Schiller, *AIP Conf. Proc.* **756**, 284-286 (2005), hep-lat/0412011.
- [22] A. Sternbeck, E. -M. Ilgenfritz, M. Müller-Preussker, and A. Schiller, *Nucl. Phys. Proc. Suppl.* **140**, 653-655 (2005), hep-lat/0409125.
- [23] M. Lüscher and P. Weisz, *Commun. Math. Phys.* **97**, 59 (1985) [Erratum-ibid. **98**, 433 (1985)].
- [24] K. Orginos, D. Toussaint, and R. L. Sugar, *Phys. Rev.* **D60**, 054503 (1999); G. P. Lepage, *Phys. Rev.* **D59**, 074502 (1999).
- [25] D. Becirevic *et al.*, *Phys. Rev.* **D61**, 114507 (2000), hep-lat/9909082.